Gas turbines in a carbon-neutral society
10th International Gas Turbine Conference
11-15 October 2021

Paper ID Number: 23-IGTC21

THE DESIGN AND OPTIMISATION OF A HYDROGEN COMBUSTOR FOR A 100 KW MICRO GAS TURBINE

Cedric Devriese*°, Willem Pennings*, Henk de Reuver*, Gijs Penninx*, Guido de Ruiter*, Rob Bastiaans*, Ward De Paepe°

*Eindhoven University of Technology, Power & Flow Group, Eindhoven, Netherlands
°University of Mons, Thermal Engineering and Combustion Unit, Mons, Belgium

PO Box 513, 5600 MB Eindhoven
+32 473 67 35 12
c.p.devriese@tue.nl

ABSTRACT

Along growing deployment of renewable electricity production, like wind and solar, the demand for energy storage will increase. One of the most promising ways to cover the medium to long-term storage is to use the excess electricity to produce hydrogen via electrolysis. Therefore, the importance of research into the design of a small to medium-sized hydrogen fueled micro Gas Turbine (mGT) unit for efficient, local heat and electricity production becomes apparent. One of the largest challenges to this end is the design of an ultra-low NOx hydrogen combustor. In this paper, we report on the progress of our work towards that goal. Firstly, an initial single-nozzle swirler (swozzle) combustor geometry was proposed and designed using steady RANS and LES. Numerical results of this swozzle combustor indicated unacceptable high NOx emissions (1400 ppm). Therefore, in a second step, a full CFD (steady RANS) design and optimization of an alternative combustion chamber concept, the micromix type which is known for its advantages towards NOx-emission reduction, was performed. This improved micromix combustor geometry resulted indeed in a NOx level reduction of more than 1 order of magnitude compared to the initial swozzle design (from 1400 ppm to 250 ppm). Additionally, several design parameters, such as the position and diameter of the hydrogen injection nozzle and the Air Guiding Panel (AGP) height, have been optimized to improve the flow patterns.

NOMENCLATURE

Acronyms

AGP	Air Guiding Panel
CFD	Computational Fluid Dynamics
CHP	Combined Heat and Power
CIM	Ceramic Injection Moulding
DES	Decentralised Energy Systems
FC	Fuel Cells
FGM	Flamelet Generated Manifolds
LAM	Laser-Assisted Machining
LES	Large Eddy Simulation
LHV	Lower Heating Value
mGT	micro Gas Turbine
NO_x	Nitrogen Oxides
OPEX	Operational Expenditures
RANS	Reynolds Averaged Navier-Stokes
RICE	Reciprocating Internal Combustion Engine
TIT	Turbine Inlet Temperature

Symbols

k	AGP height
P	Compressor outlet static pressure
T	Relative tip gap
x	Primary zone mixing length
y	Hydrogen injection depth

INTRODUCTION

Renewable energy storage, for both mid- and long term, is most feasible by using the excess electricity (e.g., strong wind on a public holiday) for electrolysis to produce green hydrogen [1,2]. However, the low volumetric energy density of hydrogen (~2.7 kWh/Nm³) [3] causes research to be focussed on converting hydrogen into other, possibly liquid forms, like ammonia or synthetic carbon-based fuels [4], especially for transport applications. Additionally, most of these fuels are so-called drop-in fuels, which means they can be used in existing combustion engines with only minor modifications. However, the low roundtrip efficiency causes many of these fuels to be priced out of the market. For example, the net overall efficiency on LHV basis, including electricity

consumption and pre-treatment, but excluding transport of biomass, is 67 % for allothermal gasification [5]. Therefore, despite lower energy density, a better option, especially for stationary applications, is to directly use the hydrogen for electrical power generation.

The green hydrogen (i.e. hydrogen produced by electrolysis from excess renewable energy) would then be used more efficiently in a small- to medium size local Combined Heat and Power (CHP) unit to produce electricity and heat directly were it is needed, instead of in a conventional, large power plant. Both in densely populated, urban, highly grid connected markets, which require supply reliability and peak shaving abilities [6.7], as in rural, more isolated grids, with typically high costs for grid connection and increasingly abundant renewable energy production [8,9], decentralised energy production is already commercially viable.

In a Decentralised Energy System (DES) setup with integrated renewable energy sources, the green hydrogen can be converted into electricity and heat by using 3 different technologies: Reciprocating Internal Combustion Engine (RICE), micro Gas Turbines (mGT) and Fuel Cells (FC). In DES applications, diesel gensets (RICE) are currently the most widely used option [10,11]. However, mGTs have a few distinct advantages when compared to RICEs. A gas turbine has only one moving (rotating) part, which leads to lower noise and vibrations levels and decreased wear on the components. This leads to much lower OPEX because the maintenance intervals are larger, and the maintenance interventions are less invasive, especially during the half-way major overhaul. The mGT also has the possibility for multi-fuel applications, opportunities for lower emissions (especially NO_x) and a cleaner exhaust [10]. When it comes to the comparison with FCs, mGTs are advantageous in many ways; they have a much higher power density, a far longer service life, the combustion process requires a less high hydrogen purity and they do not require nearly as much rare earth metals [12]. However, the main disadvantage of mGTs compared to FCs is their lower electrical efficiency. A 100 kW_e FC unit typically has an electrical efficiency of 50 %, while a current, natural gas burning mGT with the same power output only reaches 30% [10]. This explains their small market share in the small-scale CHP market [13]. An obvious solution to this problem, is running the mGT at a higher Turbine Inlet Temperature (TIT), to increase its electrical efficiency.

Currently, RICEs dominate the small-scale CHP market [14], and only a small number of mGTs (with an electrical output ranging from a few kW to 250 kW and electrical efficiencies going from 15 % to 30 %) are commercially available [15]. These units typically operate according to the recuperated Brayton cycle (see Figure 1 [15]) and they usually burn gaseous fuels (mostly natural gas). However, some are also capable of using liquid fuels like diesel, when they are equipped with a different, specific combustor. Their fuel flexibility is mostly limited. The Ansaldo-Energia T100, for instance, can only burn fuels with a Wobbe index between 43 and 55 MJ/Nm³ [16]. Additionally, and more relevant to this paper, none of these units can run on pure hydrogen. This is mainly because hydrogen combustion poses a number of difficulties, such as high flame sensitivity, a large risk of flashback and potentially high NO_x emissions [17].

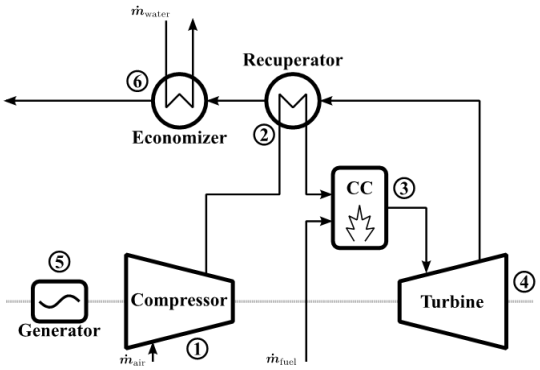

FIGURE 1: *The mGT is a typical recuperated Brayton cycle, consisting of a radial compressor (1) and turbine (4), a low-NOx burner (3), a recuperator (2) to increase the efficiency and a high-speed generator (5). Since most mGTs are used in CHP applications, the thermal power is produced in an economizer (6)*

The design of a hydrogen combustion chamber is entirely different from its natural gas burning counterpart. This is due to problems inherent with the combustion of hydrogen: problems with flame stretch, causing a more unstable flame, which can lead to flame flashback with catastrophic consequences [18] and the high adiabatic flame temperature, which causes a higher combustor liner temperature and a larger formation of thermal NO_x.

All the current experimental hydrogen, or hydrogen-mix fuel, combustor geometries for mGT applications can be divided into 3 design types:

1. The **Single nozzle with swirler design**, based on classical large-scale gas turbine combustors, uses one single centrally located nozzle and swirler for flame stabilization and gas mixing (for internal exhaust gas recirculation) in a single can. Recent examples can be found in [19-21, 17].
2. The **Multiple tangentially fired nozzle design** causes the formation of a large flame-stabilising vortex, much like design type 1, but without the need for a separate swirler. Recent examples can be found in [22, 23].
3. The **Multi-nozzle "micromix" design** uses several annular mounted smaller nozzles for jet stabilized combustion in a single can. Recent examples can be found in [24-28].

Capstone, an mGT manufacturer from the USA, has successfully used design type 2 for many years to burn methane. Experimental work has already been performed

to burn either pure hydrogen or a hydrogen-methane mix [22,23]. The most novel geometry for hydrogen combustion, however, and the design type claimed to be most beneficial for NO_x reduction, is the micromix geometry (type 3) [27]. On lab-scale, all three combustor concepts have already been tested experimentally [17,30], showing their potential in terms of flame stability and emission control.

An increase in the TIT allows to take full advantage of the potential of a hydrogen fuelled mGT, considering the higher adiabatic flame temperature of hydrogen compared to more conventional fuels, such as natural gas. As previously mentioned, the low efficiency of mGTs is the main reason behind their limited success on the market, which is mainly due to the limits on TIT. Current commercially available machines have a TIT of 950 °C, due to the temperature limitations of an all-metallic turbine [31]. With an all-metal, non-cooled turbine, a recuperator inlet temperature of 700 °C and other state-of-the art components, the expected maximal thermal efficiency is close to 30 % for a 50 kW_e mGT at nominal load [32]. In his study, Rodgers showed that TIT, together with recuperator effectiveness, are the 2 key parameters that have a major impact on the thermal efficiency of an mGT [32,33]. Since the inclusion of internal air channels for film cooling of a small radial turbine rotor is difficult, and compressor air bleeding is very detrimental to the overall mGT efficiency, since the mass flow rate the compressor delivers is already rather small, the TIT of the mGT can only be increased when thermal resistant ceramic materials are introduced. The use of these ceramic materials for the turbine rotor would allow for a higher TIT, resulting in a considerable thermal efficiency increase [35].

McDonald and Rodgers already indicated in 2003 that a ceramic recuperator and a ceramic radial turbine rotor are necessary to achieve an efficiency of 40 % in a 200 kW_e mGT. In contrast, the thermal efficiency limit of an mGT with an all-metallic turbine rotor is 35 % [35]. These high levels of electrical efficiency would allow a ceramic mGT to dramatically improve its economic competitiveness [36]. More recently, small-scale mGT demonstrator machines with ceramic radial turbine rotors, burning conventional fuels, have been made and tested [37,38]. Until a few years ago, ceramic turbine rotors could only be manufactured using conventional machining operations like grinding. This made the whole process difficult, long, and costly, allowing only simple rotor geometries. With modern techniques however, such as Laser-Assisted Machining (LAM) [39] and Ceramic Injection Moulding (CIM) [40], the manufacturing of ceramic rotors for high-speed applications is no longer only for one-off experimental machines.

Although the mGT presents itself thus as the best option to convert pure hydrogen into electricity and heat in a DES framework with CHP, several challenges, linked to the increase of TIT and the use of pure hydrogen in the combustor, still need to be overcome to increase the efficiency to make the unit competitive. With our research, we aim at finding answer/solutions to these challenges with as end-goal the design and construction of an experimental demonstrator of a 100 kW hydrogen-fuelled mGT. In this paper, we present our advances obtained during the past two years towards the **design and optimisation of a combustor system for a 100 kW hydrogen-fuelled mGT.**

This paper has two main parts. Firstly, the 1-D thermo-chemical design followed by the full CFD analysis (RANS and LES) which resulted in the initial single-nozzle swirler (swozzle) combustor geometry is presented. Since a switch towards a micromix type combustor, due to its advantages towards NOx-emission reduction, was performed, the second part presents the design and optimization of such a micromix type combustor.

"SWOZZLE" COMBUSTOR DESIGN

The main requirements of the envisaged mGT are that the net electrical output power of the gas turbine should be equal 100 kW, while the turbine inlet temperature (TIT) should not exceed 1300°C (1573 K), considering the mechanical properties of the Silicon Nitride radial turbine. Air is admitted to the combustor by a centrifugal compressor, which compresses air to a pressure of 4 bar(a). This is close to the typical maximum pressure rise for a subsonic single stage radial compressor. Moreover, this pressure is also equal to the combustor pressure of the AE-T100, a comparable natural gas fuelled mGT. Before entering the combustor, the compressed air is heated by a recuperator to a temperature of 930 K (approximately 650°C). This combustor inlet temperature was chosen as it results in a turbine outlet temperature close to, but comfortably lower than, the maximum operating temperature of the recuperating heat exchanger, namely 930°C. Given these boundary conditions, the air mass flow rate and air-to-fuel equivalence ratio can be calculated.

Air and fuel mass flow calculation

Since the TIT constraint governs the required amount of excess (cooling) air, the calculations aim to find an air mass flow for which the TIT is not exceeded. Given an electrical power output P = 100 kW, an assumed generator efficiency $\eta_g = 0.2$ and the lower heating value (LHV) of hydrogen of 119.96 MJ/kg, the required fuel mass flow m_f is 4.2 g/s. The outlet state of the combustion chamber is calculated using the previously calculated inlet states, assuming complete combustion without dissociation effects. Combustion is assumed to take place at constant enthalpy and pressure, such that the mixture enthalpy of the reactants and the products are equal. Since the temperature of the mixture of products is initially unknown, its enthalpy is calculated for a prescribed large temperature range. The output mixture enthalpy is then matched to the known input mixture enthalpy. The corresponding outlet temperature is then calculated. The

process described above is executed for a range of compressor mass flow rates while maintaining a constant fuel mass flow, allowing to determine the corresponding outlet temperature and overall equivalence ratio. The results indicate that, to satisfy the outlet temperature constraint, a compressor mass flow rate of 0.58 kg/s is required to dilute the hot primary combustion gas.

Geometry

Once the mass flow rate through the combustion chamber is determined, a first geometrical design can be proposed. In this paper we considered the design of a combustor with a can-type geometry with a design methodology mainly based on the work of Lefebvre and Ballal [41]. The can-type combustor is a simple and often used type and has the added benefit of being easy to integrate in a modular mGT layout. The geometry is configured such that 20 % of air is admitted through the centre with the remainder going through the annulus. This yields a theoretical primary zone equivalence ratio of 1.18. As such, the flame is designed to burn in a slightly fuel-rich environment to keep the flame temperature low and thereby limit NO_X formation in the primary mixing zone. However, this concept was designed for hydrocarbon fuels and not for pure hydrogen.

Several studies have characterized global pressure losses for typical combustor geometries. For a can-type combustor, Lefebvre and Ballal [41] propose a value for $\Delta p_{3\text{-}4}/p_3 = 0.07$ and a value for $\Delta p_{3\text{-}4}/q_{ref} = 37$, whereby the subscripts 3 and 4 denote the inlet and outlet of the combustor respectively and q_{ref} denotes the dynamic pressure ($\rho v^2/2$). This allows us to calculate the reference cross-sectional area of the combustor casing according to Eqn. 1 from Lefebvre and Ballal [41]:

$$A_C = \left[\frac{R}{2}\left(\frac{\dot{m}_3\sqrt{T_3}}{p_3}\right)^2 \frac{\Delta p_{3-4}}{q_{ref}}\left(\frac{\Delta p_{3-4}}{p_3}\right)^{-1}\right]^{0.5} = 0.0126 \text{ m}^2 \quad (1)$$

It is desirable for the annulus velocity to be relatively low such that the static pressure drop between the annulus and liner is sufficiently high. This is beneficial since a high pressure drop promotes dilution air penetration and mixing. An optimal value of k, the ratio of liner cross-sectional area and casing cross-sectional area is derived using Eqn. 2 from Lefebvre and Ballal [41]:

$$k_{opt} = 1 - \left(\frac{(1-\dot{m}_{sn})^2 - \lambda}{\Delta p_{3-4}/q_{ref} - \lambda r_a^2}\right)^{1/3} = 0.75 \quad (2)$$

with $r_a = A_{in}/A_C$ the cross-sectional area ratio of the combustor inlet and casing. The liner cross-sectional area then becomes:

(3)

The corresponding casing diameter D_C and liner diameter D_L then become 127 mm and 110 mm respectively.

Within the liner, several zones can be distinguished, as be seen in Figure 2. The primary mixing zone is where fuel and air are initially mixed and combusted. The secondary zone is where more air is added to finish the combustion process. Finally, in the dilution zone, more air is added to the combustion products to cool them down to an acceptable temperature.

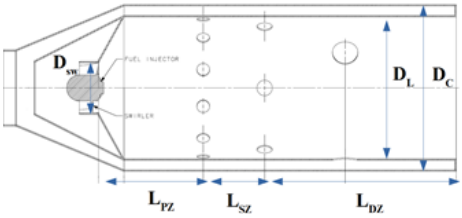

FIGURE 2: *Sketch of the preliminary swozzle combustor geometry*

The length of the primary and secondary zones can be calculated using Eqns. 4 and 5 from Lefebvre and Ballal [41]:

$$L_{PZ} = \frac{3}{4}D_L = 0.083 \text{ m} \quad (4)$$

$$L_{SZ} = \frac{1}{2}D_L = 0.055 \text{ m} \quad (5)$$

The length of the dilution zone is a function of the combustor's pattern factor (PF) and the dynamic pressure drop factor $\Delta p_{3\text{-}4}/q_{ref}$. The pattern factor is defined in Eqn. 6 from Lefebvre and Ballal [41]:

$$PF = \frac{T_{max} - T_4}{T_4 - T_3} \quad (6)$$

Since the value of T_{max} is unknown, it is assumed that PF = 0.3, a value which corresponds with those commonly found in literature [42, 43]. Melconian and Modak (as cited by Conrado [43]) have provided several curves of which the dilution zone length can be calculated as a function of PF and the dynamic pressure drop factor. Since no curve is available for $\Delta p_{3\text{-}4}/q_{ref}$ =37, it is obtained by linear interpolation of the two nearest curves. The value is also multiplied by the liner diameter to finally obtain the dilution zone length L_{DZ}. This yields a total liner length of 281 mm.

The hydrogen flames should be contained (stabilized) in the primary mixing zone of the combustor. This is accomplished by creating an area of reversed flow in which hot combustion products are constantly mixed with fresh fuel and air. In this case, a swirler (with high swirl intensity) will be used. It should be noted that alternatives to high-swirl burners exist: in more recent studies, low-swirl burners (LSBs) have shown superior emissions performance using premixed combustion with respect to classical gas turbine combustor systems [44]. The swirler area is calculated using Eqn. 7 from Lefebvre and Ballal [41]:

$$A_{sw} = \sec\theta\left(\frac{2\rho_{in}\Delta p_{sw}}{\dot{m}_{sw}^2 K_{sw}} + \frac{1}{A_L^2}\right)^{-0.5} \quad (7)$$

In this equation, Δp_{sw} is the swirler pressure loss, m_{sw} is the mass flow rate through the swirler, θ is the vane angle and K_{sw} is the so-called concordance factor. The swirler area A_{sw} is equal to the swirler annulus area minus the area occupied by the vanes, approximated by Eqn. 8 from Lefebvre and Ballal [41]:

$$A_{sw} = \frac{\pi}{4}\left(D_{sw}^2 - D_{hub}^2\right) - 0.5 n_v t_v \left(D_{sw} - D_{hub}\right) \quad (8)$$

Where D_{sw} is the outer swirler diameter, D_{hub} is the hub diameter, n_v is the number of vanes and t_v is the vane thickness. Certain choices were made for the parameters listed in the formulas above, which yields A_{sw} = 8.9E-04 m^2 and D_{sw} = 40 mm. To check whether the amount of swirl is high enough to create sufficient recirculation, the swirl number S_N is calculated. It was derived by Beer and Chigier [45] and is defined by Eqn. 9 from Lefebvre and Ballal [41]:

$$S_N = \frac{2}{3} \cdot \frac{1 - \left(D_{hub}/D_{sw}\right)^3}{1 - \left(D_{hub}/D_{sw}\right)^2} \tan\theta = 1.11 \quad (9)$$

For the swirling flow to cause recirculation, the swirl number should be higher than a critical value of $S_N \sim 0.4$ [41]. This clearly is the case, and as such, the swirler geometry theoretically satisfies the requirements.

Throughout each of the three combustion zones, the liner is perforated with holes (see Figure 2). Large holes are used to admit air for combustion and mixture cooling purposes; small holes are used to cool the liner wall. The large air admission holes increase in diameter further downstream; more and more air is admitted as combustion progresses.

Mesh and model setup

Once the initial design of the combustion chamber was finished, a full CFD analysis was performed to validate the 1-D thermo-chemical tools used to shape the geometry. The proposed geometry was discretised using the ANSYS Meshing application. A global maximum face size of 2 mm was chosen with a refinement using maximum face sizes of 0.05 mm and 0.1 mm in the fuel inlet and swirler respectively. The resulting 3D unstructured mesh containing 1.5M elements for one third of the full combustor.

The turbulence model used is the realizable k - ε model. The k - ω SST was also considered, but this would have required a finer boundary layer mesh, which would have further increased the mesh count. The solution is considered converged as soon as all residuals drop below 10^{-3}, except for the energy equation, of which the residual should drop below 10^{-6} for it to be considered converged. Initially, some equations were solved using a first order upwind scheme to improve solution stability. All equations were finally solved using a second-order upwind discretization scheme to achieve the convergence criteria. Under-relaxation factors (URFs) are adjusted as the calculation progresses to improve solution stability. The outer walls of the combustion chamber are modelled as being adiabatic. Ignition occurs there where the equivalence ratio of the mixture is equal to or greater than unity since the air enters the combustor at a temperature higher than the autoignition temperature of hydrogen.

Cold flow CFD (RANS)

The CFD study performed on the swozzle design contains three different numerical simulations; a cold flow RANS simulation, a reactive flow RANS simulation and a reactive flow LES. Cold flow analysis involves modelling of the flow through the combustor without considering combustion. This methodology allowed to build and evaluate the CFD model systematically and iteratively. Even though combustion of fuel induces significant thermodynamic changes, the cold flow results could still be used to evaluate and improve various parts of the combustor in an early stage. The swirler-induced flow recirculation can be improved or adjusted after reviewing cold flow analysis results by, for example, adjusting the swirler vane angle or adjusting the swirler mass flow. The liner hole placement strategy can also be revised based on the observed liner pressure drop, jet penetration and mixing behaviour.

Reactive flow CFD (RANS)

Fuel is initially unmixed as it is injected somewhat downstream of the oxidizer (air) inlet. Combustion is therefore predominantly non-premixed. However, pure fuel is injected which first mixes with oxidizer until the Rich Flammability Limit (RFL) is reached. As such, the fuel is slightly premixed when it is consumed in the combustion process. Considering this, the partially premixed combustion model was selected as the most suitable combustion model. It combines the non-premixed model (mixture fraction approach) and the premixed model (progress variable approach). The temperature field shows a maximum temperature, slightly downstream of the swirler near the flow recirculation zone, of 2680 K (see Fig. 3), which corresponds with the (Probability Density Function) PDF table data. The mass-weighted average temperature at the combustor outlet is 1564 K, which is 0.6 % lower than the target value of 1573 K, with maximum and minimum temperatures varying approximately +/- 200 K from the average. The NOx emissions are analysed by activation of the thermal NOx formation model. This showed a NOx mass flow rate of 0.825 g/s, which resulted in an average mass fraction of NOx at the combustor outlet of 1410 ppm. The maximum flame speed is reached at an equivalence ratio of approximately 1.8, which matches the theoretical calculations.

Reactive flow CFD (LES)

In addition to the RANS simulations, Large Eddy Simulations (LES) on the reactive flow have also been performed to model more accurately the turbulent

structures in the recirculation zone, with a finer grid resolution in this area. By coarsening the mesh further downstream and refining the mesh in the recirculation region, the 3D unstructured tetrahedral mesh on 1/3 of the combustor geometry was fine enough to capture the main vortex structures in the recirculation zone, while keeping the cell count at 1.5M.

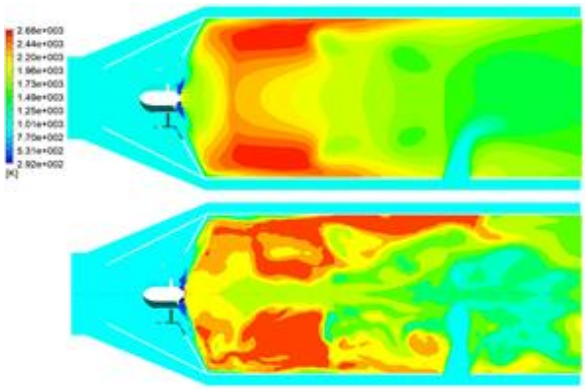

FIGURE 3: *Temperature contours in steady RANS (top) and LES snapshot (bottom) in the "swozzle" combustor geometry*

Figure 3 also shows the temperature contours of the LES results at t = 2.6 ms, which was almost identical to the time-averaged RANS temperature contours of the fully developed flow. The results clearly illustrate the difference between a RANS and LES solution as the temperature contours show much more detail than a time-averaged solution (Fig. 3). The extent to which the last dilution jet penetrates the flow is much higher with respect to the RANS solution. The transient results also show that cold and hot spots form and then dissipate again within a millisecond at the outlet of the combustor. The average combustor outlet temperature and NO_X-emissions remain nearly unchanged when compared to the steady RANS simulation.

Swozzle geometry: conclusion

An exhaust NO_x concentration of 1400 ppm is far too high even for an unoptimized geometry. Instead of spending more time on trying to get this number to a single-digit ppm value, as would be required for a modern gas turbine, it was decided to abandon this design and switch to the design and optimisation of a micromix type combustor geometry. The micromix design uses several smaller annular placed nozzles instead of one centrally placed nozzle. The recirculation caused by this setup produces a jet-stabilised flame, that promises to yield the desired ultra-low NOx emissions.

"MICROMIX" COMBUSTOR DESIGN

The micromix combustion principle was developed as a dry (i.e., without adding steam into the combustion chamber) combustion system with low NO_x pollution. Conventional dry low NO_x combustion principles are based on lean premixing and thereby lowering the combustion temperature. This, however, is not possible for hydrogen powered gas turbines due to the high flammability of hydrogen, which increases the risk of flashback (ignition before the combustion chamber, leading to uncontrolled combustion inside the combustion chamber). The micromix principle is designed to create multiple short flames instead of one big flame. This lowers the residence time in high temperature zones leading to lower NO_x emissions [46].

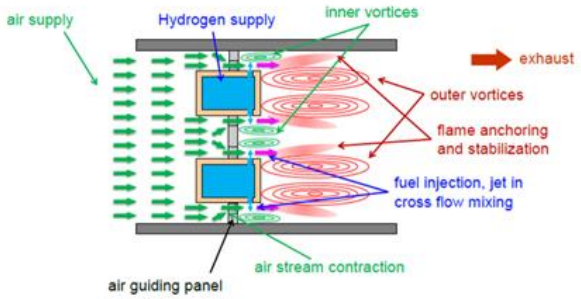

FIGURE 4: *The micromix combustion principle is based on several smaller flames, rather than one single large flame, and by doing so reducing the residence time in the high temperature zone, leading to reduced NOx emissions [47].*

The micromix principle is schematically presented in Figure 4 and is briefly discussed below. The air flows in from the left, as indicated by the green arrows. The air is contracted through multiple air holes in the Air Guiding Panel (AGP). This contraction leads to an accelerated air stream and small vortices after the AGP. Hydrogen is injected into this air stream on a 90-degree angle (jet in cross flow). Vortices also arise in the wake of the hydrogen supply ducts. These two vortices, indicated with green and red in Figure 4, stabilize the hydrogen-air mixture stream in between them, leading to a shear layer flame with low residence time. It should be avoided that hydrogen enters the re-circulation area of the inner vortices, because this will increase residence time and therefore the NO_x production. This means that the injection depth should always be smaller than the critical value $y < y_{crit}$, as can be seen in Figure 5. Extrapolating from literature data, the starting point for the design of the micromix combustor contained a total of 9 hydrogen inlet in 2 concentric rings.

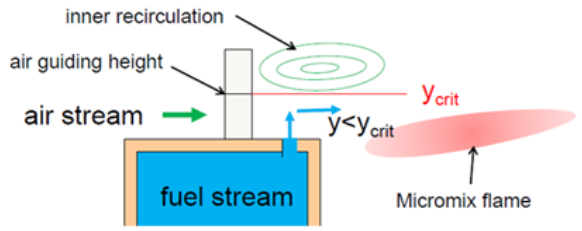

FIGURE 3: *Highlighting the maximal injection depth, to avoid hydrogen from entering the inner recirculation vortex [47]*

Numerical setup

The combustion problem is solved using Reynolds-averaged-Navier-Stokes equations (RANS), with a mass flow inlet boundary condition for the air (0.0022 kg/s) and hydrogen (2.58772 e-5 kg/s) flows and a static pressure outlet boundary condition of 400000 Pa. Turbulence is modelled using a realizable k-ε model with enhanced wall treatment. The combustion model used was the standard Fluent Equilibrium Chemistry Model with Partially Premixed Combustion and the Decoupled Detailed Chemistry Model, to be able to predict NO_x-emissions. In this model, the formation of thermal NO_x is determined by the extended Zeldovich mechanism. The basic solver convergence criteria are based on the solution residuals. These are set to 1e-6 for the energy equation and 1e-3 for all other transport equations. Additionally, a convergence monitor on the mass flow-averaged temperature in the entire domain was used to check the convergence of the temperature distribution in such a way that the average temperature should not change by more than 1K over 50 iterations. This usually leads to residuals 10^{-4} for all transport equations.

In this work, the CFD simulations were focussed on analysing the differences between several combustor geometries, rather than an in-depth discussion of the combustion properties of a single combustion chamber type. In this context, the choice for the realizable k-ε model with enhanced wall treatment was made as it provided a way to compare several different combustor geometries with a limited computational cost.

To perform a calculation in the entire reaction zone, which is approximately 15 cm long, starting from the hydrogen supply duct, an element size of 10 µm would lead to a computational cost that was beyond our capacity. To be able to perform a grid study, the problem is scaled down to a small part of the total geometry, which is based on symmetry and covers all important mixing and reaction phenomena. This method was also used by Ayed et al. [47] to study the effect of design parameters to the micromix principle. The computational domain covers a longitudinal burner slice which makes use of both radial and tangential symmetric configuration of the burner. The radial boundaries represent the middle of a hydrogen supply duct and the middle of an air guiding panel. The tangential boundaries are set at the middle between two hydrogen injectors and through the centre of one hydrogen injector. A first domain for the combustor geometry was proposed and will later be updated after the first CFD simulations. A 2D slice of this domain can be seen in Figure 6.

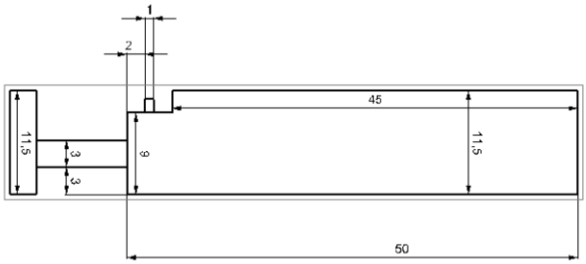

FIGURE 6: *2D slice of the computational domain of our initial micromix geometry*

An initial grid sensitivity analysis was performed on 3 increasingly finer meshes to find a sufficiently large mesh for this simulation. The main element size was set to 0.5 mm for all three meshes, which was proven sufficiently small for the regions outside the main mixing area. A refinement was made in the entire reaction zone, which is 15 cm long, starting from the hydrogen supply duct, and close to the walls. The mesh sensitivity analysis parameters are shown in Table 1.

	Refinement cell size [mm]	Main cell size [mm]	Number of cells
Mesh A	0.25	0.5	2.5e5
Mesh B	0.125	0.5	1.4e6
Mesh C	0.1	0.5	2.5e6

TABLE 1: *Combustor mesh sensitivity analysis parameters*

The performance of the different meshes is assessed based on the temperature and mixture fraction predictions.

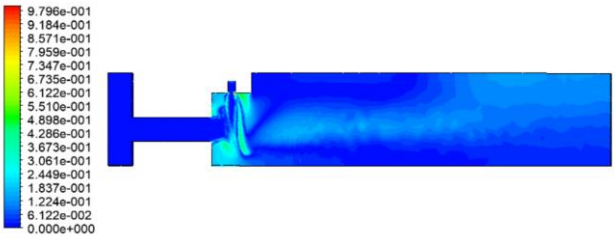

FIGURE 7: *Temperature difference between mesh A and B, as a fraction of the temperature in mesh B*

The difference in temperature between mesh A and B, as can be seen in Figure 7, reaches up to 50% of the examined temperature in mesh B in the beginning of the main reaction zone. Hence, it can be concluded that the element size of mesh A is not small enough, as further mesh refinement leads to major changes in temperature.

Both the temperature and the mixture fraction differences are negligibly small in the main flame zone,

when comparing mesh B and C (Figures 8 and 9). Both variables show bigger deviation in the zone where the hydrogen jet directly meets with the air stream. These deviations are about 5% for both the temperature and the mixture fraction. However, this region is so small that the effect of this deviation to other variables such as NO_x formation is negligibly small, especially since the temperature is relatively low in this region. It can therefore be concluded that mesh B and C perform equally well. This means that the element size used in mesh B is sufficiently small for this problem and will be used for the first simulation on our initial micromix geometry and for the subsequent optimisation.

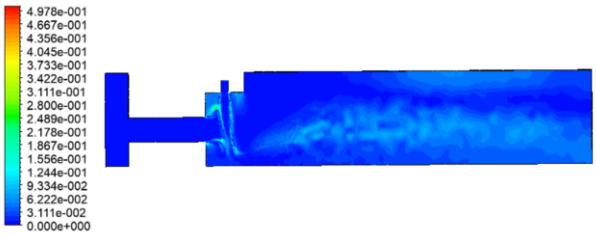

FIGURE 8: *Temperature difference between mesh B and C, as a fraction of the temperature in mesh C*

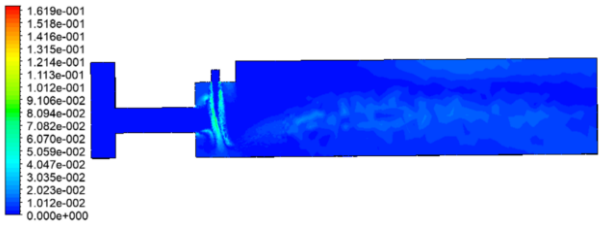

FIGURE 9: Mixture fraction difference between mesh B and C

Optimisation of our initial micromix geometry

Comparing the obtained velocity streamlines (Figure 11) from the initial geometry (design presented in Figure 6) and the desired micromix flow pattern (Figure 10), it is clear that the initial design does not yield the desired flow pattern. The injection depth is too larger which causes both poor mixing performance and a greatly reduced size of the inner vortex pair. The hydrogen jets merge to one hydrogen flow in the middle. It can also be seen that there is no real outer vortex pair created, which is probably due to the radial distance between the air guiding hole and the hydrogen supply duct. This is not only a waste of space; it also takes away the bluff-body function of the hydrogen supply duct which creates the outer vortices.

These two problems, being the excessive hydrogen injection depth and the absence of an outer vortex pair, can be solved by applying following design alterations:

1. The hydrogen injection depth needs to be lowered. This can be done by lowering the radial speed of the hydrogen jet, i.e., enhancing the hydrogen injector diameter or lowering the hydrogen mass flow per nozzle.
2. There can be no radial distance between the air guiding panel and the hydrogen injection port, in order to create better outer vortices.

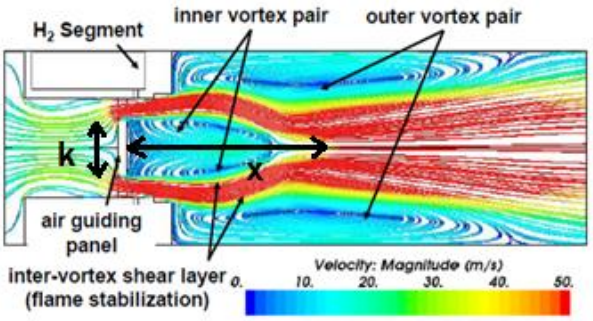

FIGURE 10: *Desired micromix flow pattern [47]*

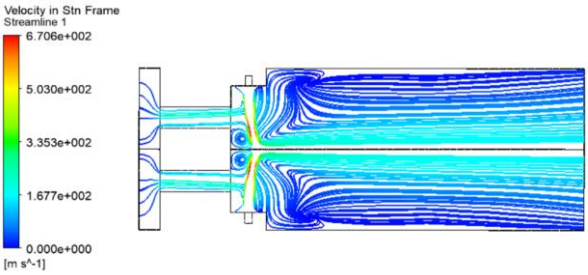

FIGURE 11: *Velocity streamlines in the first micromix proposed geometry do not correspond to the desired velocity, leading to bad performance*

Two additional design parameters, being the variation of the mixing length (x) and the Air Guiding Panel (AGP) height (k) (see Figure 10 for the location of x and k), were proposed by Ayed et al. [47] to optimize the NO_x reduction performance of the combustor

First, the mixing length variation aims to give better mixing performance which will lower the peak temperatures in the flame. Better mixing leads to lower equivalence ratio peaks in the reaction zone, leading to lower flame temperatures. Lower flame temperatures lead to lower NO_x production. Thus, a larger mixing length leads to lower NO_x emissions. The goal of the AGP height variation is to create larger inner vortices. This means that the shear layer between the inner and outer vortex pair becomes longer and that more heat is released in the primary shear layer flame fragment. This will degrade the post shear layer flame fragment size, where a large part of the NO_x formation takes place [47].

Based on these findings, a second, improved micromix geometry was proposed and studied. The mixing length has been increased and the AGP height has been lowered. Moreover, the radial distance between the air guiding hole and the hydrogen supply duct has been entirely removed. The hydrogen and air stream velocities proposed by Ayed et al. [47] for a micromix combustor with hydrogen inlet pipe diameter of 1 mm are 200 m/s and 100 m/s respectively. Hence, the hydrogen mass-flow was reduced and the air guiding holes are enlarged to reach

these velocities. In reality, this would mean an increase of the number of hydrogen jets in the combustion chamber, since the total fuel mass flow rate of the combustor design is fixed. The air mass flow rate has also been scaled to the corresponding amount of air guiding holes

Finally, analysis of the initial single nozzle-swirler design found that the local equivalence ratio (1.18) is far too high for the micromix principle to work properly. It was found by Ayed et al. [47] that at a local equivalence ratio of about 0.4, stable and distinct micromix flames are formed for a hydrogen injector diameter of 1 mm. Hence, the air mass flow was enhanced to this local equivalence ratio of 0.4.

CFD analysis of the improved micromix geometry

Using the same numerical setup as presented in previous section, both the flow pattern (Figure 12), NO mass fraction and temperature distribution (Figure 13) of the final micromix geometry could be obtained. A clearly separated micromix flame has formed, in the range of about 15 mm starting from the hydrogen supply duct, as was expected (see Figure 10). The shear layer and post shear layer flame fragments can be identified as well in the high temperature zones in Figure 13. The NO_x emissions at the outlet are an order magnitude lower than in our previous single-nozzle swirler design (125 ppm versus 1400 ppm). However, it is still 2 orders of magnitude higher than the micromix reference case [47], which has NO_x emissions below 5 ppm. Note that NO_x predictions are represented as raw values in the exhaust and not at dry conditions at 15% O_2, due to the fact that we did not do this for the swozzle design either, allowing for direct comparison. Our final micromix combustor should certainly have single digit NO_X emissions, so we must keep improving our design towards that goal

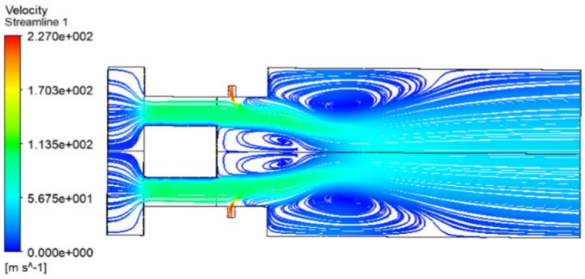

FIGURE 12: *Velocity streamlines in the improved micromix geometry, showing good resemblance with the desired velocity profile*

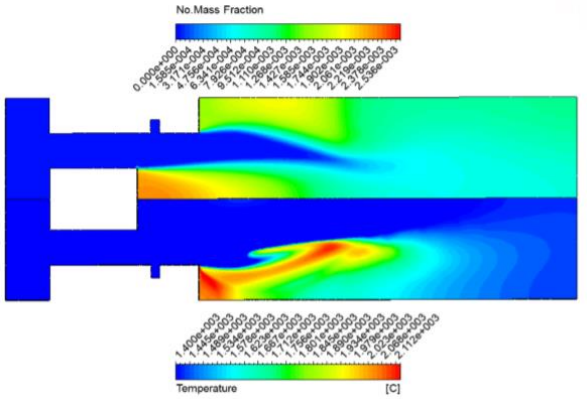

FIGURE 13: *Temperature and NO mass fraction in our improved micromix geometry*

CONCLUSIONS AND FUTURE WORK

In the route towards the design and construction of a 100 kW hydrogen-fuelled mGT demonstrator unit, in this paper, we presented the CFD-based design of the combustion chamber. In this work, more specifically, the initial steps for the development, including a first swozzle design and later an improved and optimized Micromix design were presented, and the numerical simulation results are discussed.

The CFD RANS simulation results indicate clearly that the micromix geometry is indeed superior compared to the swozzle design regarding NOx emissions. Moreover, we are gradually improving the performance of our combustor design exploiting this Micromix principle to eventually reach the single digit NOx exhaust ppm, which will be necessary to comply with current regulation. To that end, the next step is twofold. First, a continued optimisation effort of the micromix design, based on both detailed chemistry and FGM combustion models. Secondly, a small-scale experimental setup of the primary combustion and mixing zone to experimentally validate the CFD simulations performed for this paper.

ACKNOWLEDGEMENTS

The first author acknowledges the support of Fonds de la Recherche Scientifique – FNRS.

REFERENCES

[1] "Energy storage – the role of electricity", European Commission Staff Working Document, Brussels, 1.2.2017 SWD(2017) 61 final

[2] A. Van Wijk. "The Green Hydrogen Economy in the Northern Netherlands", The Northern Netherlands Innovation Board, April 2017

[3] K. Müller, J. Geng et al. "Reversible vs. Irreversible Conversion of Hydrogen: How to Store Energy Efficiently?," Energy Technology, vol. 1, pp. 42–47, 2013.

[4] M. Bailera, P. Lisbona et al. "Power to Gas projects review: Lab, pilot and demo plants for storing renewable energy and CO2," Renew. Sustain. Energy Rev., vol. 69, pp. 292–312, 2017.

[5] Christiaan M.van der Meijden, Hubert J.Veringa et al. "The production of synthetic natural gas (SNG): A comparison of three wood gasification systems for energy balance and overall efficiency", Biomass and Bioenergy Volume 34, Issue 3, March 2010, Pages 302-311 Biomass and Bioenergy

[6] Ralph Sims, Antonio Pflüger et al. "Contribution of Renewables to Energy Security: IEA Information Paper", Renewable Energy Working Party, March 2007, Section 3

[7] Bernard F. Kolanowski. "Guide to Microturbines", Fairmont Press, 2004, p.42

[8] Diego Silva Herran, Toshihiko Nakata. "Design of decentralized energy systems for rural electrification in developing countries considering regional disparity", Applied Energy Volume 91, Issue 1, March 2012, Pages 130-145

[9] Martin Pehnt, Martin Cames et al. "Micro Cogeneration: Towards Decentralized Energy Systems", Springer-Verlag Berlin Heidelberg, 2006

[10] Frost & Sullivan, 2011. "Combined heat and power: Integrating biomass technologies in buildings for efficient energy consumption."

[11] B. Metz, O.R. Davidson et al. "Contribution of Working Group III to the Fourth Assessment Report of the Intergovernmental Panel on Climate Change", IPCC Fourth Assessment Report: Climate Change 2007, Section 4.3.8

[12] Sossina M. Haile. "Materials for fuel cells", Materials Today, Volume 6, Issue 3, March 2003, Pages 24-29

[13] Technavio. "Global Gas Turbine Market 2016-2020", May 2016

[14] "Diesel Generator Market Size, Share & Trends Analysis Report By Product (Low Power, Medium Power, High Power), By End Use (Residential, Commercial, Industrial), By Region, And Segment Forecasts, 2013 – 2022", Grand View Research Report, July 2018

[15] De Paepe, W., Montero et al. 2017, "Towards Higher Micro Gas Turbine Efficiency and Flexibility-Humidified mGTs: A Review," ASME J. Eng. Gas Turbines Power (Accepted for publication: GTP-17-1371, 10.1115/1.4038365)

[16] Ansaldo Energia s.p.a, 2016. AE-T100 Micro Turbine-Natural Gas. Online available: http://www.ansaldoenergia.it/easyUp/file/ansaldo_aet100_natural_gas.pdf

[17] D. Mira, O. Lehmkuhl et al. "Numerical Investigation of a Lean Premixed Swirl-Stabilized Hydrogen Combustor and Operational Conditions Close to Flashback", ASME Turbo Expo 2018, GT2018-76229

[18] A. Kalantari, V. McDonnel et al. "Towards Improved Boundary Layer Flashback Resistance of a 65kw Gas Turbine With a Retrofittable Injector Concept", ASME Turbo Expo 2018, GT2018-75834

[19] Norihiko Iki, Osamu Kurata et al. "NOx Reduction in a Swirl Combustor Firing Ammonia for a Micro Gas Turbine", ASME Turbo Expo 2018, GT2018-75993

[20] Raffaela Calabria, Fabio Chiariello et al. "A Biogas Fuelled Micro Gas Turbine Using Dual-Fuel Approach", ASME Turbo Expo 2018, GT2018-76667

[21] Alex Frank, Peter Therkelsen et al. "Investigation of the Down-Scaling Effects on the Low Swirl Burner and its Application to Microturbines", ASME Turbo Expo 2018, GT2018-77208

[22] Kalb, Drosser et al. (2009). Emission characteristics of premixed cyclic-periodic-mixing combustor operated with hydrogen-natural gas fuel mixtures, JEngr Gas Turbine Power, Vol 132(2) 021505

[23] Therkelsen, Werts et al. (2009). Analysis of NOx formation in hydrogen-fueled gas turbine engine, J. Engr Gas turbines and Power (2009), Vol 131(3),031507

[24] Stefan Hasemann, Hannah Seliger et al. "Experimental and Numerical Design Study for a Small Scale Jet-Stabilized Micro Gas Turbine Combustor", ASME Turbo Expo 2018, GT2018-75050

[25] Timo Zornek, Thomas Mosbach et al. "Optical Measurements of a LCV-Combustor Operated in a Micro Gas Turbine With Various Fuel Compositions", ASME Turbo Expo 2018, GT2018-75481

[26] Xunwei Liu, Weiwei Shao et al. "Investigation of H2/CH4-Air Flame Characteristics of a Micromix Model Burner at Atmosphere Pressure Condition", ASME Turbo Expo 2018, GT2018-76276

[27] Ramzi Ben Abdallah, Vishal Sethi et al."A Detailed Analytical Study of Hydrogen Reaction in a Novel Micromix Combustion System", ASME Turbo Expo 2018, GT2018-76586

[28] H. H.-W. Funke, J. Dickhoff et al. "Experimental and Numerical Study of the Micromix Combustion Principle Applied for Hydrogen and Hydrogen-Rich Syngas as Fuel with Increased Energy Density for Industrial Gas Turbine Applications", The 6th International Conference on Applied Energy – ICAE 2014-863

[29] Lee, McDonell et al. (2011). Ultralow emissions hydrogen/syngas combustion with a 1.3 MW injector using a micromixing lean premixed system, Paper GT2011-45929.

[30] York, Ziminsky et al. (2013). Development and Testing of a Low NOx Hydrogen Combustion System for Heavy-Duty Gas Turbines, J. Engr Gas Turb Power, Vol 135(2), 022001

[31] Nickel Institute."Engineering Properties of ALLOY 713C"

[32] C. Rodgers, Microturbine cycle options, in: ASME Conference Proceedings, 2001, ASME paper 2001-GT-552, p. 10 pages.

[33] C. F. McDonald. "Recuperator considerations for future higher efficiency microturbines", Applied Thermal Engineering 23 (2003), 1463-1487.

[34] L. Goldstein, B. Hedman et al. "Gas-Fired Distributed Energy Resource Technology Characterizations", National Renewable Energy Laboratory, Oak ridge, Tennessee, U.S.A., 2003.

[35] C. F. McDonald, C. Rodgers, "Ceramic recuperator and turbine: The key to achieving a 40 percent efficient microturbine", 2005, ASME paper GT2005-68644

[36] S. Campanari, E. Macchi, "Technical and tarif scenarios effect on microturbine trigenerative applications", Journal of Engineering for Gas Turbines and Power 126 (2004) 581-589.

[37] Takeshi Sakida, Shinya Tanaka et al. "Development of the Ceramic Gas Turbine Engine System (CGT301)", ASME 1999 International Gas Turbine and Aeroengine Congress and Exhibition, Volume 1: Aircraft Engine; Marine; Turbomachinery; Microturbines and Small Turbomachinery, June 7–10, 1999

[38] Colin F. McDonald, Colin Rodgers. "Small recuperated ceramic microturbine demonstrator concept", Applied Thermal Engineering 28 (2008) 60-74

[39] Harsha Panuganti. "Understanding fiber-coupled diode laser superheating in laser-assisted machining [LAM] of silicon nitride (Si3N4)", August 2009

[40] Powder Injection Moulding International. "Ceramic Injection Moulding used to produce high performance gas turbine components", September 16, 2016

[41] A. H. Lefebvre and D. R. Ballal, Gas turbine combustion: alternative fuels and emissions. CRC Press, third ed., 2010.

[42] C. P. Mark and A. Selwyn. "Design and analysis of annular combustion chamber of a low bypass turbofan engine in a jet trainer aircraft", Propulsion and Power Research, vol. 5, no. 2, pp. 97-107,2016.

[43] A. C. Conrado, P. T. Lacava, et. al. "Basic Design Principles for Gas Turbine Combustor" Proceeding of 10th Brazilian Congress of Thermal Sciences and Engineering, 2004.

[44] D. Yegian and R. Cheng. "Development of a Lean Premixed Low-Swirl Burner for Low NOx Practical Applications", Combustion Science and Technology, vol. 139, no. 1, pp. 207-227, 1998.

[45] J. Beer and N. Chigier. "Combustion Aerodynamics". London: Applied Science Publishers, 1st ed., 1972.

[46] S Boerner, et al. "Development and integration of a scalable low NOx combustion chamber for a hydrogen-fueled aerogas turbine". EUCASS Proceedings Series – Advances in AeroSpace Sciences, 4:357–372, 2013

[47] A.H. Ayed. "Numerical Characterization and Development of the Dry Low NOx High Hydrogen Content Fuel Micromix Combustion for Gas Turbine Applications". PhD thesis, Aachen University of Applied Sciences, 2017

[48] C. Devriese, et al. "The Preliminary CFD Design of a Compressor and Combustor System Towards a 100 kW Hydrogen Fuelled Micro Gas Turbine". ASME Turbo Expo 2019, GT2019-91342